Alma Mater Studiorum · University of Bologna

Fermilab Summer School
07/31/17 - 09/29/17

The Muon g-2 experiment: Laser Calibration System

Author:
Paolo Girotti

Supervisor:
Marco Incagli

Abstract

The new Muon g-2 experiment at Fermilab will measure the anomalous magnetic moment a_μ of the positive muon with a precision of 140 parts per billion. This measurement is motivated by the result of the Brookhaven Laboratory experiment that in 2001 showed a 3.5 standard deviation discrepancy with the standard model prediction with a precision of 540 ppb. This experiment has several improvements, one of these is a laser calibration system for all the 1296 channels of the 24 calorimeters. My objective during this summer internship was to implement a calibration mode called *double pulse* that allows a study on the calorimeter response when two positrons hits the detector at the same time. The majority of the work was on the hardware, since I helped mounting and aligning the optics, soldered and prepared several cables used to control motorized mirrors, connected a Delay Generator to the NIM electronics and to the lasers. I also worked both on the software necessary to analyze the data and to communicate remotely with the devices located in the Laser Hut. Now the setup is ready and fully functioning, and some runs have been executed. At the end of my program, I also prepared and hosted an exhibit representing the Laser Calibration System to be shown to the $\sim$5000 people that came to Muon g-2 during the big Fermilab Open House event for the 50th anniversary.

Contents

Chapter 1

Muon g-2

1.1 The "g" in g-2

The magnetic dipole moment $\vec{\mu}$ of an object is a measure of how much torque it experiences when placed in a magnetic field:

$$\vec{\tau} = \vec{\mu} \times \vec{B} \tag{1.1}$$

Subatomic particles have a magnetic moment that is generated by their intrinsic angular momentum (spin). According to the Dirac quantum theory [1], the magnetic moment of a point-like, spin $\frac{1}{2}$ particle is given by:

$$\vec{\mu} = g\frac{Qe}{2m}\vec{S} \tag{1.2}$$

where the dimensionless g factor is exactly equal to 2. Actually, the real value of g differs from 2 by small amounts due to interactions of the particle with virtual particles in vacuum. The contributions of the standard model theories in the case of muons are given by eq. 1.3.

$$g_{SM} = 2_{Dirac} + \mathcal{O}(10^{-3})_{QED} + \mathcal{O}(10^{-7})_{QCD} + \mathcal{O}(10^{-9})_{EW} \tag{1.3}$$

The difference between the real value of g and 2 is called *anomalous magnetic moment* and calculated as:

$$a = \frac{g-2}{2}$$

The simplest higher order interaction is the QED "Schwinger interaction", that contributes for exactly $\frac{\alpha}{2\pi}$. In the case of electrons, QED interactions are basically the only anomalous processes.

Since other interactions involving new particles contribute to g-2 proportionally to $(m/M_\chi)^2$, where m is the mass of the lepton and M_χ the mass of the virtual particle, in order to find new physics the muon is the perfect particle to study.

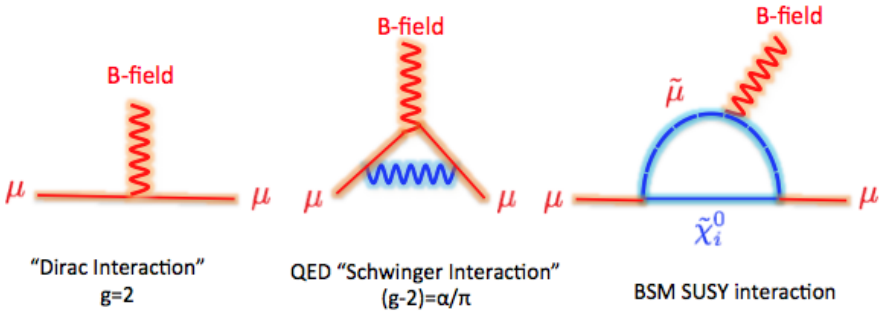

Figure 1.1: Feynman diagrams of the interactions between muons and virtual particles.

1.2 The experiment

The Brookhaven National Laboratory g-2 experiment named E821 has left us with a 3.5σ discrepancy with the standard model prediction of $a_\mu = 11\,659\,180.4(5.1) \cdot 10^{-10}$. It measured a value of

$$a_\mu = 11\,659\,208.0(5.4)(3.3) \cdot 10^{-10}$$

with a precision of 540 ppb [2].

The new Muon g-2 experiment at Fermilab aims to improve the precision of the same measurement, using 21 times the number of muons. This increase in statistics, together with improvements in systematic uncertainty, could provide an accuracy of 140 ppb and a $> 7\sigma$ discrepancy from the SM if central value is confirmed [3].
It is composed of a 15 m diameter circular superconducting magnet, that can produce a very uniform magnetic field of 1.45 T, and a set of 24 calorimeters and trackers placed on the inside of the ring to observe the positrons produced by the muons. The magnet is the same one that was used in the BNL experiment, and it was moved via sea and land in an operation called *The big move*.

1.2.1 How it works

The anomalous magnetic moment is a very interesting property of muons to be studied, because it can be predicted by theory with very high accuracy and at the same time can be measured as precisely in an unambiguous experimental setup. The muon g-2 experiments observe the motion of the spin of the muons that travel in circular orbits in a homogeneous magnetic field. Since it is crucial to know the spin direction of the muons when they enter the magnet, it is necessary to have them polarized. Fortunately, the process that produce positive muons comes in our help: charged pions decay produce polarized muons due to the parity violation in weak interaction.

$$\pi^+ \to \mu^+ \nu_\mu$$

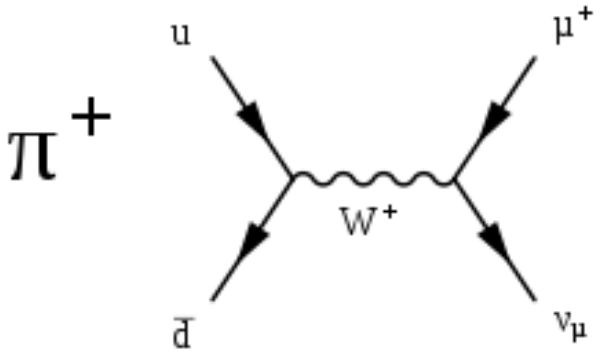

Figure 1.2: Feynman diagram of the π^+ decay.

Given the fact that right-handed neutrinos ν_R are not produced in the weak transitions mediated by the charged $W^{\pm}$ gauge bosons, only ν_L neutrinos are emitted. In the center of mass reference the products of the decay (μ^+ and ν_μ) are emitted back to back. In order to conserve the angular momentum, along with the left-handed helicity state of the neutrinos, the μ^+ must be left-handed as well. Since pions are spin 0 particles, muons should be emitted isotropically, but given that pions are relativistic and the solid angle covered by the beam pipe is small, the muon beam results very polarized.

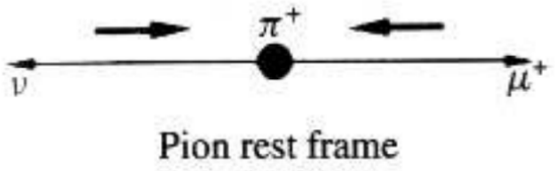

Figure 1.3: Direction and helicity of the products of pion decays.

Positive pions are produced at Fermilab by accelerating protons and smashing them into a fixed target. The resulting pions then travel inside the Muon Delivery Ring, decaying into muons with a branching ratio of 0.999877 [4]. Finally, this very clean beam of muons enters the Muon g-2 storage ring with a momentum of 3.094 GeV/c, then decaying after several revolutions into positrons. While muons travel inside the ring, their spin precess around the magnetic field direction. The spin precession frequency is given by Larmor and Thomas equation:

$$\omega_s = \frac{eB}{m}\left(\frac{g-2}{2} + \frac{1}{\gamma}\right) \tag{1.4}$$

where γ is the Lorentz factor. By removing the cyclotron frequency given by

$$\omega_c = \frac{eB}{m\gamma} \tag{1.5}$$

we obtain the anomalous frequency ω_a, calculated as

$$\omega_a = \omega_s - \omega_c = a_\mu \frac{eB}{m} \tag{1.6}$$

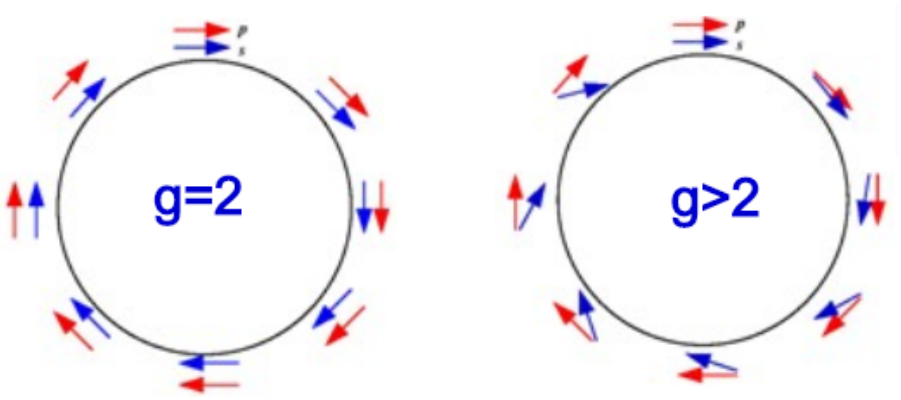

Figure 1.4: Thanks to the anomalous magnetic moment, the spin of muons precesses faster than it would do with g=2.

To have a measure of a_μ, it is sufficient to precisely measure ω_a and $\vec{B}$. In order to have a focused beam of muons, in the experiment is also present a quadrupole electric field, so that the equation becomes

$$\vec{\omega}_a = \frac{e}{m}\left[a_\mu \vec{B} - \left(a_\mu - \frac{1}{\gamma^2 - 1}\right)\vec{v} \times \vec{E}\right] \tag{1.7}$$

It seems also that a measure of $\vec{E}$ is necessary, but interestingly it is possible to choose the so called *magic momentum* so that $\frac{1}{\gamma^2-1} = a_\mu$, that is $\gamma = 29.3$, corresponding to the value of 3.094 GeV/c.

The muons decay via a three body weak decay, as shown in figure 1.6.

$$\mu^+ \rightarrow e^+ \nu_e \bar{\nu}_\mu$$

Once again, the parity violation of weak interactions assures that a left-handed neutrino ν_{e_L} and a right-handed antineutrino $\bar{\nu}_{\mu_R}$ are produced in the massless approximation. There are two possible configurations for this decay: one with the positron emitted in the

direction of the muon spin, the other in the opposite direction. In both cases the neutrinos are emitted opposite to the positrons and thanks to the parity violation their spin sum is 0. In order to conserve the angular momentum, in the first configuration the positron will be right handed, in the other case it will be left handed. By helicity conservation, the right handed positron is very preferred. Therefore the emitted positron will be

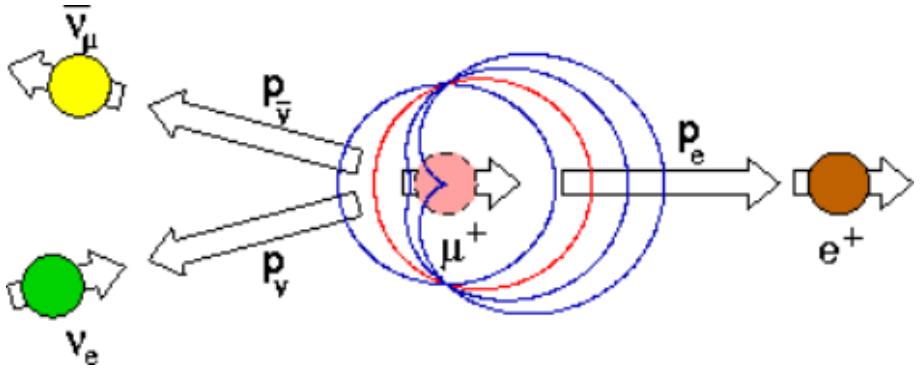

Figure 1.5: Preferred decay mode of positive muon. The positron will be emitted mostly in the muon's spin direction.

preferably emitted in the same direction as the muon's spin (fig 1.5). A measurement of the direction of the positron momentum then provides the direction of the muon spin. So, by measuring the position and time of the detected positrons it is possible to finally obtain the anomalous spin precession frequency ω_a. This is done by the experiment with a set of 24 very fast calorimeters.

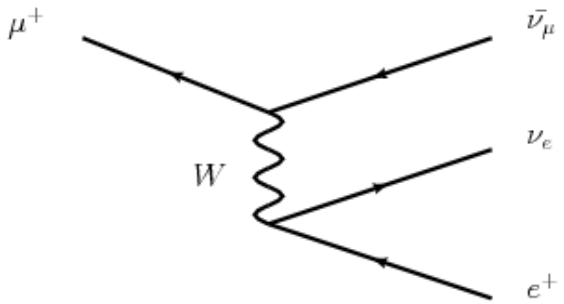

Figure 1.6: Feynman diagram of the μ^+ three body decay.

1.3 Calorimeters

Each calorimeter station is a 9 wide by 6 tall array of individual crystals. Each crystal is a 14 cm long lead fluoride (PbF_2) block with a square cross section of side 2.5 cm. While this kind of calorimeter has not been extensively used in the past, its properties are particularly well suited to the needs of the Muon g-2 experiment: PbF_2 has very high density (7.77 g/cm^3), a 9.3 mm radiation length and a Molière radius of $R_M^E = 22$ mm for energy deposition. Incoming positrons deposit energy in each crystal by emitting Cherenkov radiation in few nanoseconds, and a large area SiPM encodes the light signal in a fast charge pulse. These 54 signals are recorded using custom 12 bit 800 MHz waveform digitizers, and read out using a GPU-based data acquisition system [7]. Their purpose is to measure the energy of the positron - to have an energy threshold, and to precisely measure the time of detection - to have a measure for ω_a.

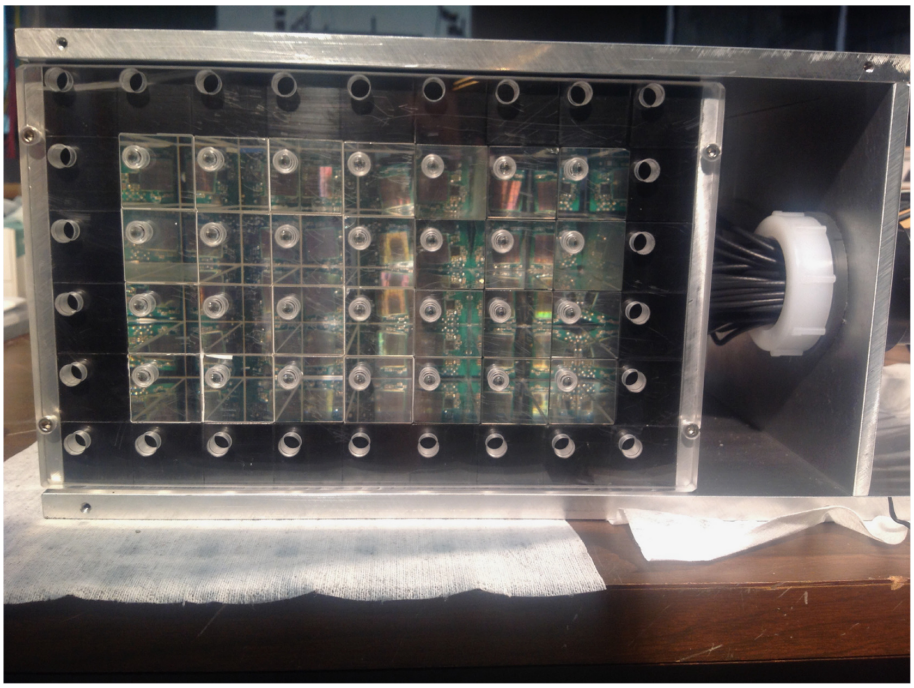

Figure 1.7: Calorimeter prototype tested at SLAC. Here it was used a smaller setup with 7x4 crystals.

Chapter 2

Laser Calibration System

In order to have a very precise measurement, it is required to have a very frequent calibration of the 24 calorimeters. Knowing their energy and time response and the gain stability over time is crucial for a successful experiment.
To do so, a setup of 6 lasers and proper optics has the job to periodically send light pulses to all the calorimeters via 25 m long quartz fibers. All the optics is located in a black interlocked room called Laser Hut, placed just outside the storage ring. Each laser sends light to 4 fibers using mirrors and splitter cubes, and all the 24 fibers exit the Hut to reach the calorimeters.

2.1 Calibration of the laser

In order to calibrate the calorimeters, we first need to know how much light we are sending through the fibers. Each calorimeter splits the light incoming by diffusing it to 55 fibers: 54 go to the crystals, and the remaining one is sent back to the Laser Hut. A set of 24 PMTs (Local Monitors) then convert the light of these returning fibers into electronically readable signals. Since the PMT response is linear, the PMT signal is expected to be proportional to the number of photoelectrons, $n_{p.e.}$:

$$\mu - \beta = k\langle n_{p.e.}\rangle \tag{2.1}$$

where μ is the mean of the PMT pulse integral distribution, after the baseline subtraction β. The signal variance is shown in eq 2.2 and it is the sum of a photoelectrons statistics term ($\sigma^2_{p.e.}$), an electronic noise contribution (σ^2_e), and the intrinsic laser pulse fluctuations ($\sigma^2_L = (\alpha k(\mu - \beta))^2$), where α is the average relative laser intensity variation, which has been measured to be less than 1%.

$$\sigma^2 = \sigma^2_{p.e.} + \sigma^2_e + \sigma^2_L \tag{2.2}$$

Since the photoelectrons component follows the Poisson statistics, assuming a statistical independence of the three sources of fluctuations, it is possible to write σ^2 as a function of the measured light intensity:

$$\sigma^2 = k^2\langle n_{p.e.}\rangle + \sigma_e^2 + \sigma_L^2 = k(\mu - \beta) + \sigma_e^2 + q(\mu - \beta)^2 \tag{2.3}$$

The proportional factor k can be obtained by fitting the plot σ^2 versus $(\mu - \beta)$ with a *pol2* function, and it is the conversion factor from pulse integral and photoelectrons seen by the PMT. In fact, we can use this factor to calculate the photoelectrons as

$$N_{p.e.} = \frac{\mu}{k} \tag{2.4}$$

To conduct this kind of study, we want to send light with different luminosity to the PMTs. Each laser is then equipped with a motorized filter wheel, that holds several filters with different transmission factors.

2.2 Data analysis

For this study six different filters have been used, and we executed one run for each filter, with several laser pulses each. The null filter (100% transmittance) is used twice, at the beginning and at the end, to check if there is any fluctuation in the PMT gain during the hours of the runs. No visible difference is found and distribution means are comparable.

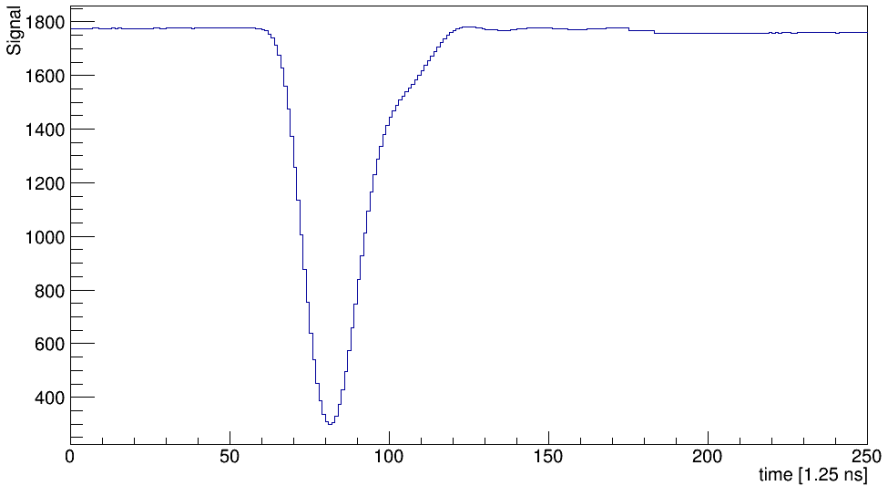

Figure 2.1: Typical signal recorded by a Local Monitor PMT.

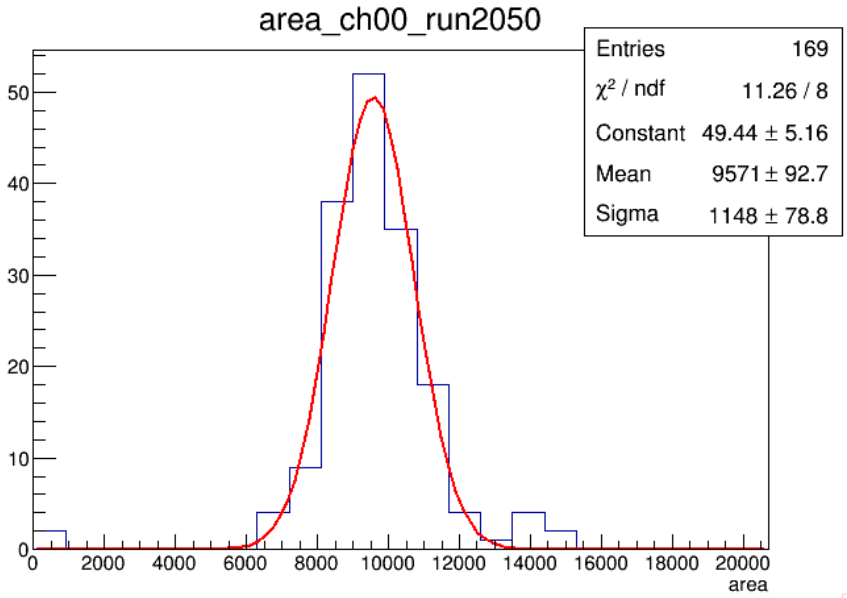

Figure 2.2: Distribution of the integrated area of a PMT signal, the one corresponding to calorimeter number 0. A gaussian fit shows μ and σ.

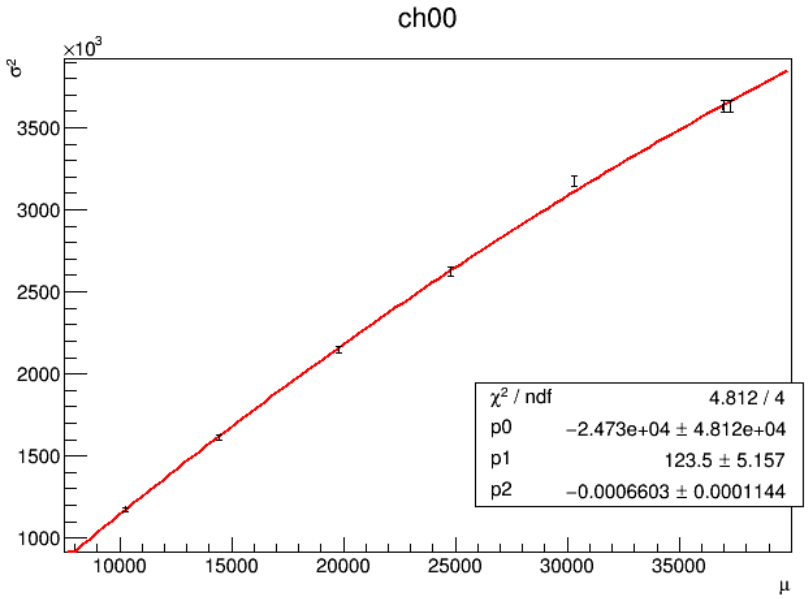

Figure 2.3: σ^2 vs μ plot for calorimeter 0, with each point representing one filter. Pol2 fit shows the linear parameter k.

As shown in figure 2.3, a value of $k = 124 \pm 5$ is found for calorimeter 0. That means that for no filter (100% transmittance), the number of photoelectrons is roughly $N_{p.e.} = \mu/k = 37000/124 \sim 300$ p.e.
In addition, a systematic negative value of $p2$ is found for each calorimeter. This is not what we expect from theory, and the cause may lie in a saturation caused by too high operating voltages for the PMTs.

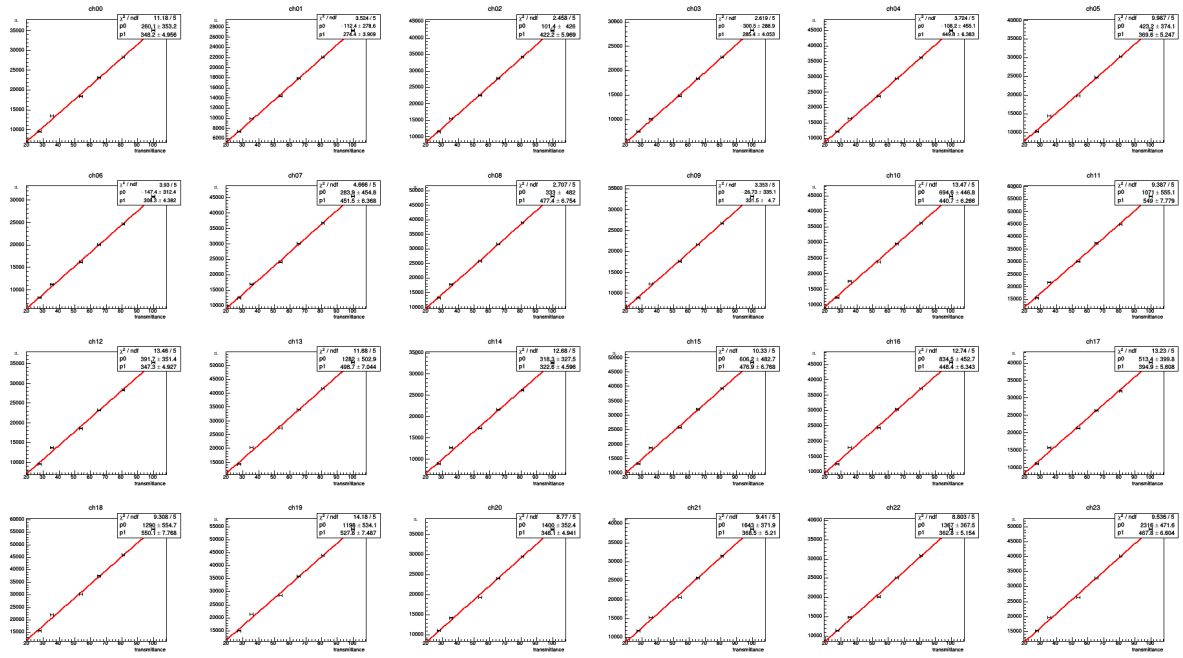

Figure 2.4: μ vs filter transmittance plot for each calorimeter for a linearity study. A linear fit (pol1) is applied.

Finally, a study on the linearity response of the PMTs have been done. As shown in figure 2.4, where μ vs transmittance is plotted for each calorimeter, we find a strong linearity, so that our assumptions in section 2.1 were correct.

Chapter 3

Double Pulse

With the laser calibration system we also want to study the calorimeter response to two really close (in time) positrons hitting the detector. This study is performed to check if it is possible to resolve signal pile-ups even at the nanoseconds scale, other than to analyze the gain response of the SiPMs in such events. The analysis of the gain response, shown in fig 3.1 necessary to study the double pulse effects on the energy threshold of the positrons.

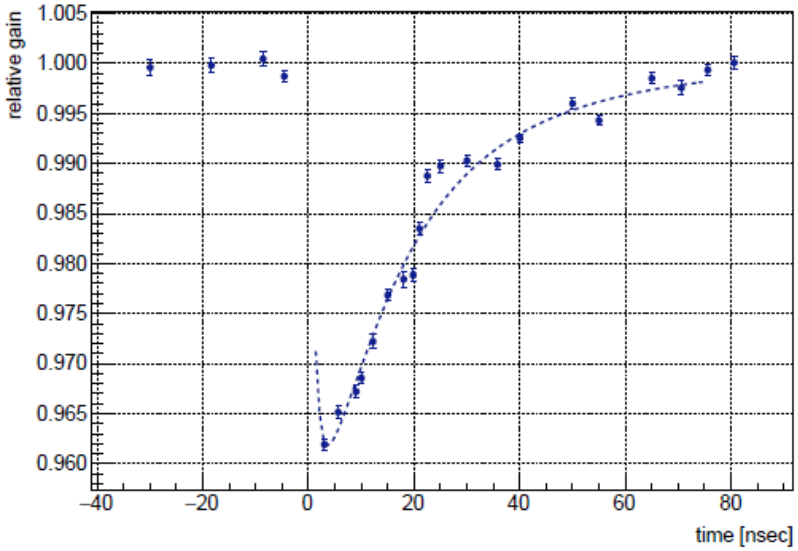

Figure 3.1: Relative gain of the laser pulse with respect to a reference LED pulse versus a fixed time interval between the two pulses [6].

The main goal of my work in the two months of the summer school was to make this possible.

3.1 Optical table

First of all, I helped upgrading the optical table adding the new optic pieces necessary to deliver two lasers beams to the same calorimeters. A set of 12 fixed and 6 movable mirrors has then been placed and aligned. As shown in picture 3.3, this design allows to fire the laser number two into the same fibers that are usually lighted up by laser number one, and vice-versa. The same pattern is replicated also on the other laser pairs 3-4, 5-6. Since a single laser cannot fire with accuracy two pulses so close in time, this is the only way to have the desired double pulse. Therefore each time only half of the calorimeters can be reached by light (the ones respectively targeted by the odd and even lasers), and so the double pulse requires two independent runs.

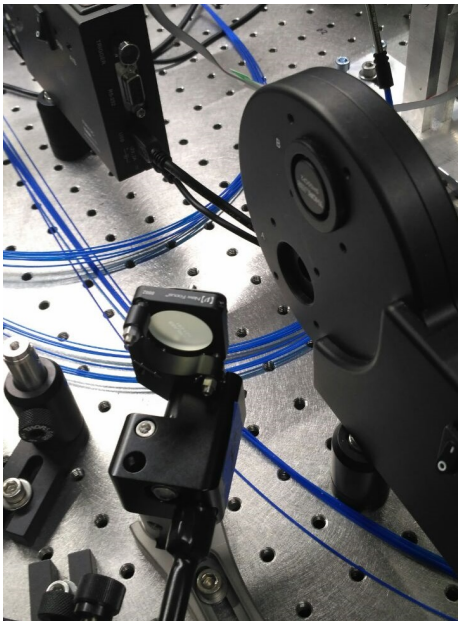

Figure 3.2: Motorized mount used to move the mirrors in and out from the light path. On the right, a motorized filter wheel.

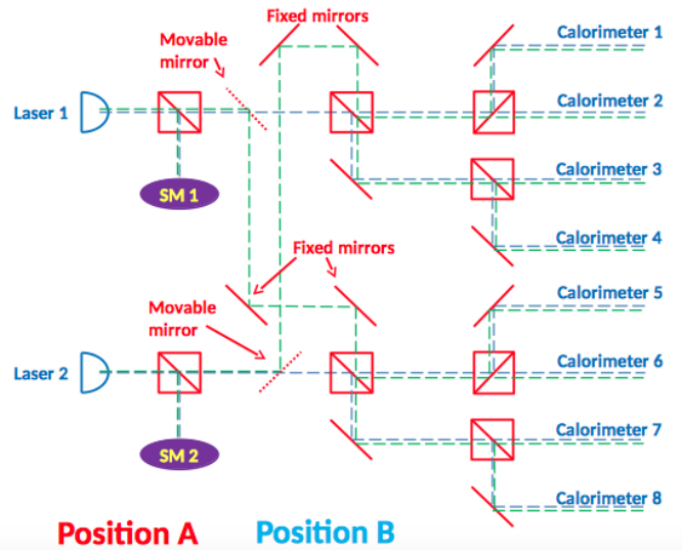

Figure 3.3: Double pulse laser setup.

In order to have the possibility to choose which laser mode (normal or double pulse) to use at any time, one motorized mirror is placed in front of each laser. They are simple flip flops that can place or remove the mirror from the light path. They have a switch pad with a button to flip their position, and they can also be controlled with external TTL signals.

So, to have a remote control, six TTL-232RG USB-to-TTL cables have been prepared and plugged in. Each cable uses a serial communication, and it has an USB plug on one

end and 6 open wires on the other end. To move the mirrors, only two wires are needed: the black one (GND, Ground) and the green one (RTS, Request-To-Send). Since the cable provides a voltage of 5 V, it is possible to generate a TTL signal using the RTS bit of the serial communication. As shown in figure 3.4, I soldered those two wires to a coaxial plug and insulated the others. The USB ends of the cables are connected to a 7-port USB hub, connected to a control pc located in the Laser Hut.

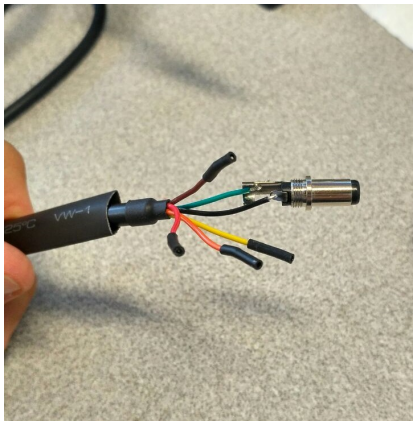

Figure 3.4: Open wires end of one cable. Black and green wires are soldered to a 2.5mm co-axial plug

Figure 3.5: The six USB-to-TTL cables are plugged into the same USB hub.

Finally, I coded a C++ driver so that it is possible to control the position of the mirrors remotely from the Muon g-2 control room. Connecting to the control pc via ssh, it is possible to launch the program and then interactively move each mirror individually or in groups. In the typical scenario, one wants to move all the odd or even mirrors simultaneously.

3.2 Delay generator

Then I worked on a Digital Delay Generator, a device that, provided an external trigger, is capable to generate a pattern of pulses with very precise delays, with a resolution of less than 100 ps. This device is necessary to fire two lasers a few nanoseconds apart.

The trigger is given by the Laser Control Board, a module of the Naples NIM crate, at a rate of about 10 Hz. The output is given by two separate channels, named AB and CD, one for each pulse of the double pulse. Of course, we want to be able to control the device remotely, in order to change the internal settings, including the delays. This device supports TCP/IP communication, so we connected it to the mini-pc with an Ethernet cable. In particular, I coded a driver in C/C++ so that it is possible to reprogram the settings from the control room, both with interactive commands and bash scripts. This

```
[laserhut2@laserhut2> ./Laser
 ----- Driver to control laserhut mirrors - PGirotti -----
 | Usage: enter laser number and position                 |
 | Laser numbers: 1,2,3,4,5,6,e,o,a  (even, odd, all)     |
 | Positions: 0,1 (down, up)                              |
 | Enter 0 to close                                       |
 ----------------------------------------------------------

 |1      |2      |3      |4      |5      |6      |
 |up     |up     |up     |up     |up     |up     |

[e 0
 Moving even mirrors down
 |1      |2      |3      |4      |5      |6      |
 |up     |down   |up     |down   |up     |down   |
```

Figure 3.6: Screenshot of the interactive display of the driver on a terminal inside the control room.

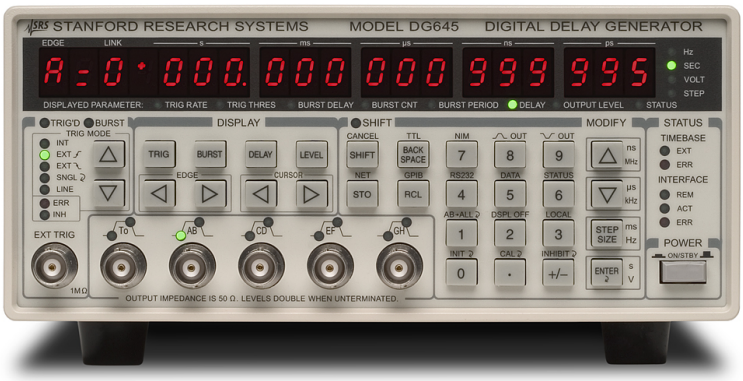

Figure 3.7: Front panel of the Delay Generator (DG645).

is necessary to change the delays automatically for the double pulse run, and to set a particular mode named *burst mode* that allows multiple pulses for each trigger. Typical delays range from 1 to 300 nanoseconds.

3.3 Electronics

The two output channels of the Delay Generator must then fire all the six lasers. This is done using some NIM modules, namely using two 4-channel FAN IN/FAN OUT modules. The first channel of both modules is used to replicate the output signals from the Delay Generator three times. Then, the copies of the first pulse go to each one of the remaining channels of the first NIM module, and the copies of the other pulse go to the remaining module. Here, the FAN IN/OUT modules are used as OR gates, where the other input comes from the Laser Control Board (LCB). The outputs finally reach the device that actually fires the lasers (SEPIA). Thanks to this setup, it is possible to fire the lasers both from the LCB and from the delay generator without moving any cable. The full diagram is shown in figure 3.8.

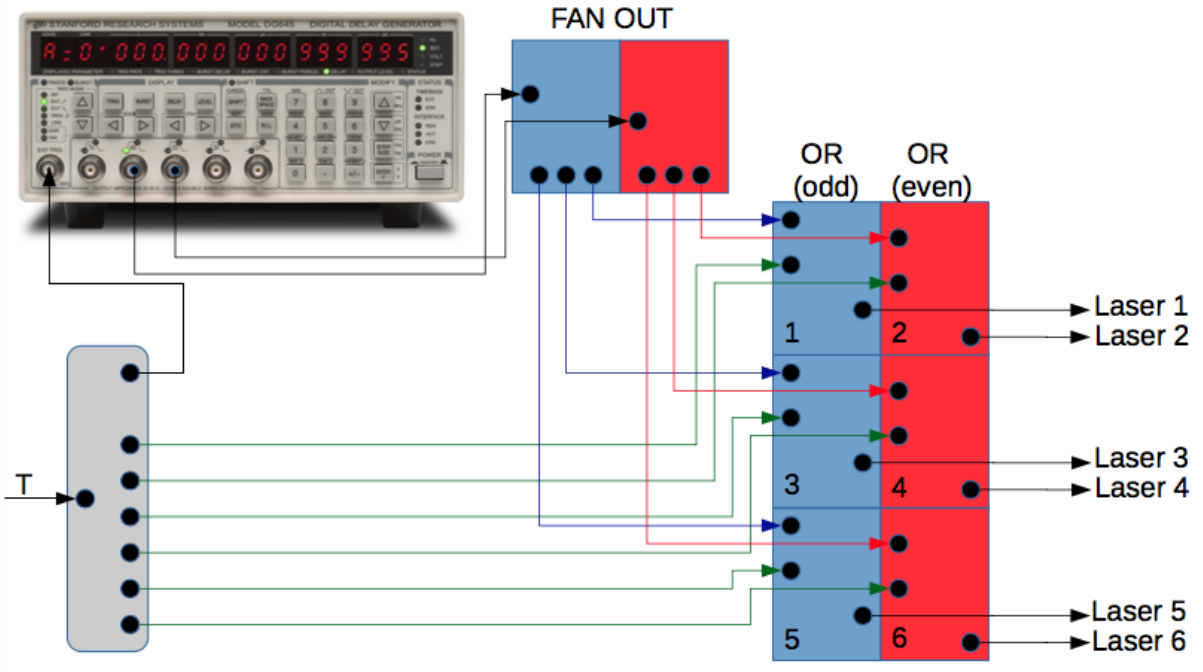

Figure 3.8: Schematic of the NIM circuit used to send the signal from the Delay Generator to the lasers.

3.4 DAQ

The whole setup is controlled from the DAQ software, that fires the lasers, opens the DAQ window, triggers the Delay Generator and records the data coming from PMTs and calorimeters. In the case of these calibration runs, each run is composed of several events, each one containing one or more laser pulses in a 700 μs "fill" window. A full structure of the trigger is shown in figure 3.9, where it is possible to see that we have 16 fills each 1.4 seconds.

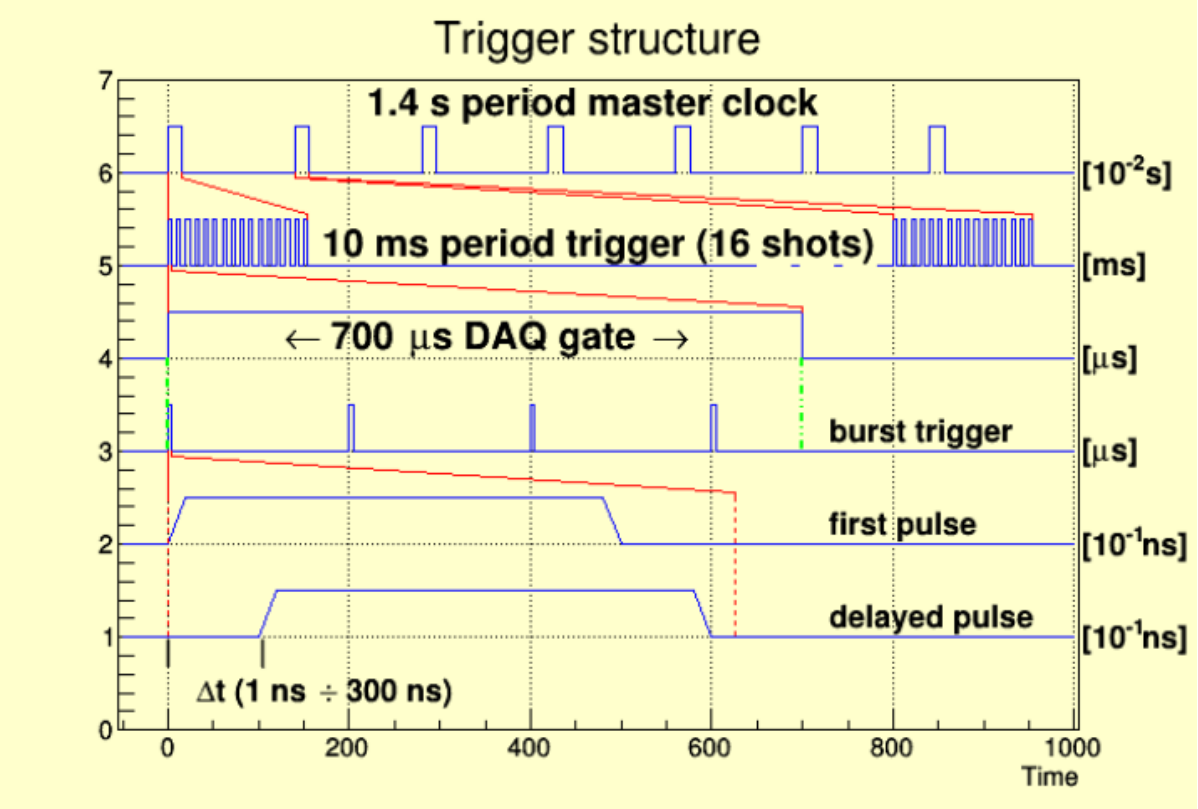

Figure 3.9: Trigger structure of the double pulse mode.

In the double pulse mode, each run represents a single delay between the two pulses. In order to coordinate the run execution and the Delay Generator reprogramming, a sequencer has been prepared. In figure 3.10 is shown a screenshot of that sequencer, with coded pulse delays ranging from 0 to 40 ns. Each run lasts 60 seconds, so that about 3000 double pulses are fired for each delay.

Data analysis

Unfortunately there were no time for me to complete the gain and response analysis of the double pulse system, also because changes of the g-2 analysis software were needed. However the setup is now completed and functional, and a full run with delays from 0 to 40 ns has been made for future analysis.

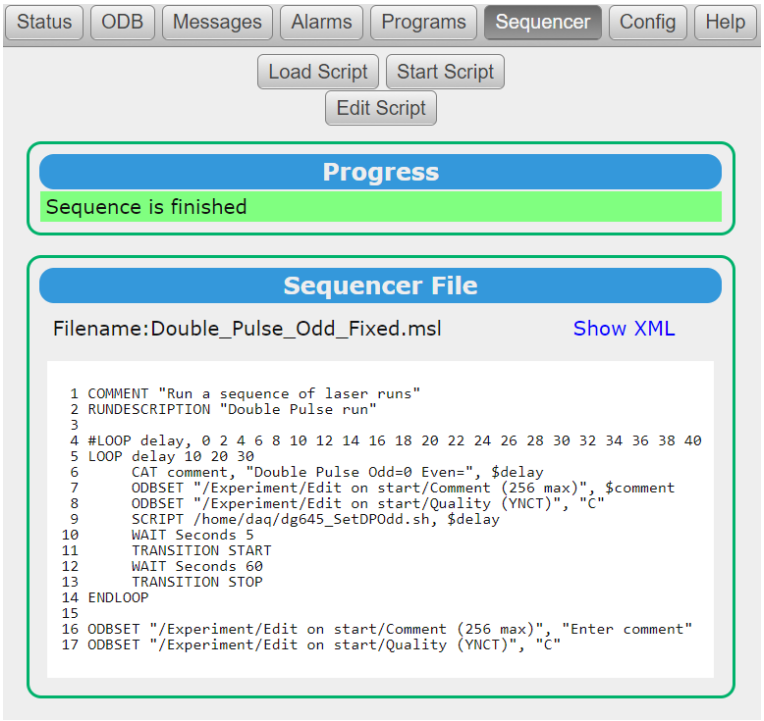

Figure 3.10: Screenshot of the sequencer that coordinates the double pulse runs.

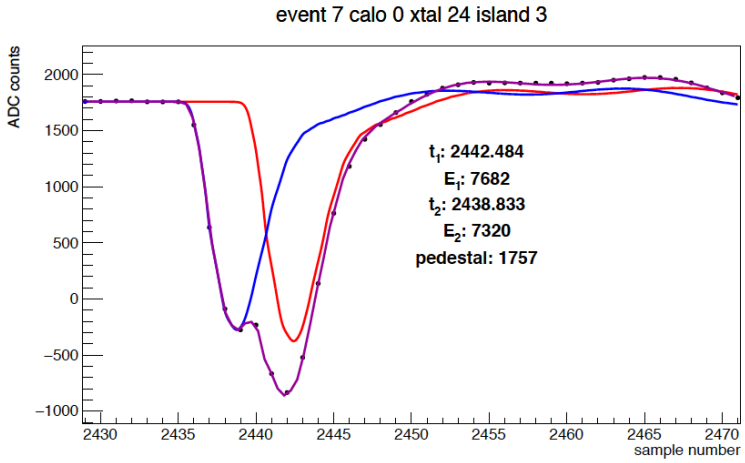

Figure 3.11: Typical double pulse signal shape for a delay of 4 ns between the pulses. A template fit is overdrawn.

Chapter 4

Fermilab Open House

This year Fermilab turned 50, and a huge public event has been organized with more than 10'000 people participating on September 23. The Muon g-2 experiment had its own exhibition, allowing the visitors to enter also into the magnet room. Many posters, videos, demos and display cases were arranged, and I contributed to this event by building a laser curio. Since the laser is closed inside the Laser Hut, the plan was to build a smaller version of the laser calibration system with real components, and to allow the public to visually and physically interact with it. We decided to have a simple setup with a laser and some mirrors to mimic the actual laser system. A red laser pointer fires a light beam that gets divided by a cube splitter (fig 4.1). The laser is controlled by an external button that the public can push (fig 4.2).

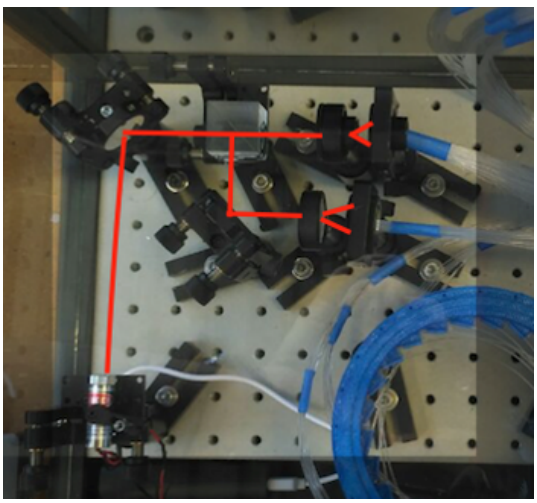

Figure 4.1: Photo from above of the optical setup. Laser path is drawn on top.

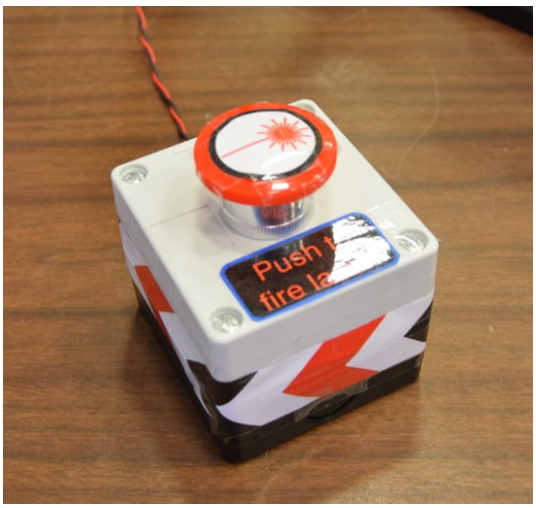

Figure 4.2: The button located outside of the display case that fires the laser.

Each one of the two resulting beams go through a diffuser. One beam lights a bundle of 24 plastic fibers connected to a 3D printed model of the magnet ring. Each fiber is glued to a piece of Plexiglas, representing a calorimeter. The other beam lights a bundle of 54 fibers connected to a panel (the same one as those of the experiment) with 54 prisms, used to bring light to the individual crystals of a calorimeter.

The people really enjoyed the event and the fact that our exhibit was interactive, as lasers are always funny. I had the opportunity to host the display case, so I explained the device and its utility for the experiment to around ∼600 people.

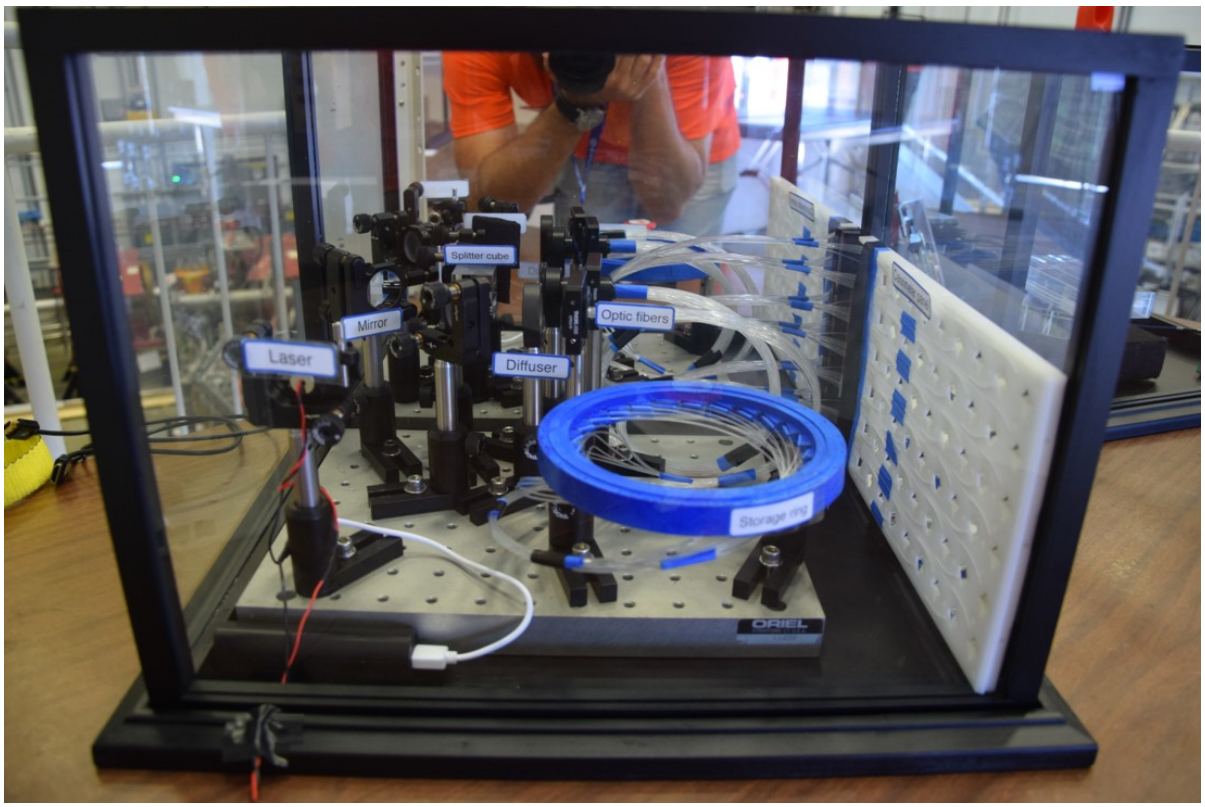

Figure 4.3: Photo of the entire display case prepared for the event.

Chapter 5

Conclusions

This experience was unique for me. I learnt a lot, both in the hardware and the software world, and I now understand what it means to work in such a rich environment as an international collaboration is. It is very satisfying to know that I contributed, yet in small part, to this important experiment. I didn't expect to have all this manual work, but that turned very stimulating and interesting, and it helped me to understand what I really like to do in physics: to project, build, operate and analyze particle detectors. Nonetheless, the Open House experience was an incredible opportunity to show and increase my passion for science-divulgation, and to talk to those many families and kids was just amazing.

I would finally like to thank all the Italian colleagues from the Muon g-2 collaboration I had the honor to work with, for the sympathy and the professionality they brought to the workplace. I learned a lot from them and I hope to work together with them again in the future.

Bibliography

[1] Paul A.M. Dirac. *The Quantum theory of electron.* Proc.Roy.Soc.Lond., 1928.

[2] G.W.Bennett et al. *Final Report of the Muon E821 Anomalous Magnetic Moment Measurement at BNL.* arXiv:hep-ex/0602035v1, 2006.

[3] W. Gohn. *The MUON g-2 EXPERIMENT AT FERMILAB.* arXiv:1611.04964v1, 2016.

[4] C. Patrignani et al (PDG). *Review of Particle Physics.* Chin. Phys. C, 40, 2016.

[5] L.P. Alonzi et al. *The Calorimeter System of the new muon g-2 experiment at Fermilab.* Nucl.Instrum.Meth. A824 (2016).

[6] J.Kaspar et al. *Design and performance of SiPM-based readout of PbF2 crystals for high-rate, precision timing applications.* arXiv:1611.03180v2, 2016.

[7] W. Gohn. *Data Acquisition for the New Muon g-2 Experiment at Fermilab.* J.Phys.Conf.Ser., 2015.